Journal of Nonlinear Science and Applications

Heat flux performance in a porous medium embedded Maxwell fluid flow over a vertically stretched plate due to heat absorption

N. F. M. Noor[a,*], Rizwan Ul Haq[b], S. Abbasbandy[c], I. Hashim[d,e]

[a]Institute of Mathematical Sciences, Faculty of Science, University of Malaya, 50603 Kuala Lumpur, Malaysia.

[b]Department of Mathematics, Capital University of Science and Technology, Islamabad 44000, Pakistan.

[c]Department of Mathematics, Imam Khomeini International University, Ghazvin, 34149-16818, Iran.

[d]School of Mathematical Sciences, Universiti Kebangsaan Malaysia, 43600 Bangi, Selangor, Malaysia.

[e]Research Institute, Center for Modeling & Computer Simulation (RI/CM&CS), King Fahd University of Petroleum & Minerals, Dhahran 31261, Saudi Arabia.

Communicated by A. Atangana

Abstract

Heat absorption and thermal radiation effects in a non-Newtonian fluid on a vertical stretching sheet with suspended particles are considered. The nonlinear partial differential equations are reduced to nonlinear ordinary differential equations via similarity approach. The equations are further solved using shooting-RK4 method and validated with homotopy-Padé solutions. Comparison between previous and present results revealed agreement up to five significant figures. The influence of various parameters on the flow velocity, temperature and concentration are examined. The profiles of reduced skin friction coefficient, Nusselt number and Sherwood number against selected parameters are sketched and discussed. Streamlines of the flow for different Maxwell parameters are visualized too. It is proclaimed that the heat flux of the flow is uplifted as value of either heat absorption or thermal radiation is multiplied. ©2016 All rights reserved.

Keywords: Maxwell, thermophoresis, homotopy-Padé, shooting, heat absorption, thermal radiation.
2010 MSC: 35Q30, 76D10, 80A20.

1. Introduction

Based on the law of conservation of energy in physics, energy is an entity that cannot be originated nor demolished but it can be transferred or transformed into diverse forms via medias around. A body

*Corresponding author
Email address: drfadiya@um.edu.my (N. F. M. Noor)

that posses energy experiences a proportional change in mass/momentum to satisfy Einstein's mass-energy equivalence [2] for static objects or energy-momentum equivalence for dynamic objects. Absorption is one of normal mechanisms of how a particular energy can be converted into another form. Energy absorption has wide applications in heat exchanger systems of automotive, machinery and reactor, metal suspension in bridge and building constructions, in material reactions such as laser and nuclear, in automated anti icing and retractor systems, and in shock absorber systems especially for permanent crash control, security and transportation safety barriers design and manufacturing. For viscous fluid flows, heat absorption is included in the energy equation to further discourse thermal distribution of the flows.

Most industrial applications of convective heat and mass transfers are based on non-Newtonian fluids. The Maxwell fluid, being the simplest subclass of the non-Newtonian models is the first viscoelastic rate type fluid which still in research favor. A Maxwellian fluid flow due to impulsively started plate is considered by Fatecau and Fatecau [4]. Concurrently they also provided a new exact solution for a Maxwell fluid on an infinite plate [5]. Sakiadis flow based on upper-convected Maxwell (UCM) fluid on a fixed plate is investigated by Sadeghy et al. [25] and they concluded that an increment in Deborah number affects the wall skin friction to decrease. On the other hand, a homotopy series solution for a magnetohydrodynamics UCM fluid flow is provided by Hayat and Sajid [12] while a unidirectional flow of an incompressible viscoelastic Maxwell fluid along an infinite permeable plate is examined by Wang and Hayat [28]. Fatecau et al. [3] concluded that the velocity profiles of an unsteady fractional derivative Maxwell fluid flow tend to be similar with the velocity profiles of ordinary Maxwell model if α tends to 1. Previous literatures on Maxwell model include heat transfer analysis for a UCM fluid flow on a horizontal stretching surface [1, 22], the mass transfer [10], the chemical reaction species [9] and the MHD channel flow embedded in a porous medium with radiation effects [13].

Thermophoresis is a phenomenon of suspended micro sized particles migration in a non-isothermal gas towards declining thermal gradient direction [9, 10, 13, 22]. Thermophoretic velocity and force are experienced by the particles as a result of temperature differences [11, 14]. Being an effective tool for collecting particles on surfaces surrounding by low temperature environment, it has abundance applications such as in microelectronics control clean room, modification of chemical/material depositions, air circulation and sampling of aerosol particles, formation in heat exchangers and particles removal from combustion systems of exhaust gases [24]. Thermophoresis is also an important mechanism in the study of semi-conductor technology especially in MHD energy generation system operations as well as in controlled high-quality wafer production [24]. A pioneer study on the nature of thermophoresis in the behavior of a laminar fluid flow over a surface with hot/cold convective conditions is conducted by Goren [6].

The homotopy analysis method (HAM) is an established analytical method inspired by Liao [16]. Ever since, this method has been widely employed to many problems of fluid flow and heat transfer, cf. [17, 23, 29]. Some recent developments of HAM include the new technique of the homotopy analysis method (nHAM), the spectral homotopy analysis method (SHAM), the Tau and homotopy analysis method (THAM) and the optimal HAM. The nHAM was proposed by reconstructing the second order nonlinear differential term of the deformation equation into two differential equations of first order [8]. In SHAM, Motsa et al. [21] blends Chebyshev pseudospectral method with HAM aspects while Shaban et al. [26] initiated THAM in the construction of shifted Chebyshev functions and their operational matrices to solve higher order deformation equations. Unlike the conventional HAM, the optimal HAM with averaged residual error can give better approximation with faster convergence [19]. Currently, the homotopy-Padé technique is employed in a limit analysis of circular plates [15] and in a real life epidemic model of smoking habit in Spain [7]. Surprisingly, the homotopy-Padé scheme seems to have better approximation property than the optimal HAM as reported by Liao [18]. Thus the objectives of the present paper are firstly to study the effects of internal heat absorption and thermal radiation in heat transfer enhancement of the Maxwell fluid flow, secondly to perform a shooting technique with fourth order Runge-Kutta method in the extended model solution and finally to validate the numerical solutions obtained with results produced by homotopy analysis method aided with Padé series acceleration.

2. Problem formulation

2.1. The governing equations and conditions

Let a steady magnetohydrodynamic Maxwell fluid flowing along a vertical stretching plate in a porous medium of Darcian type as clearly visualized in Fig. 1. A typical magnetic field B_0 is imposed normal to
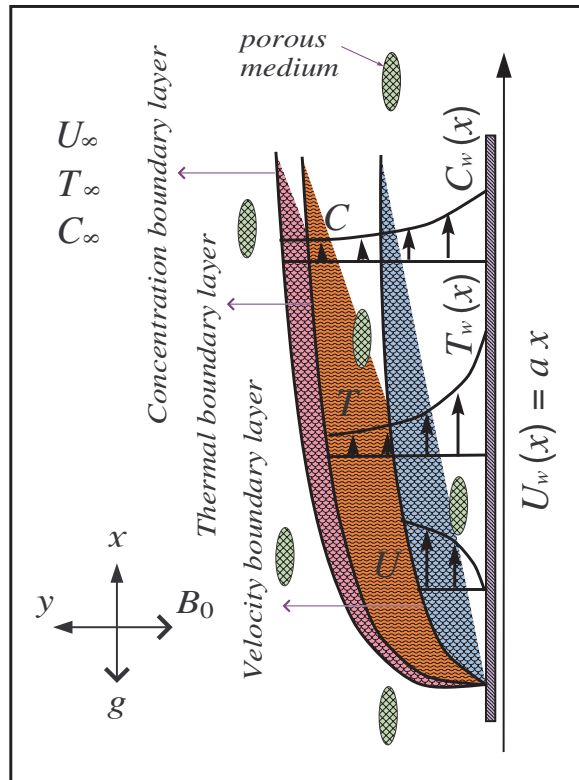

Figure 1: Geometry of the Maxwell model over a vertical surface embedded in a Darcian porous medium.

the flow direction so that the magnetic field distribution is uniform along the plate. The magnetic Reynolds number is taken to be sufficiently small such that the induced magnetic field can be ignored in regard to the applied magnetic field. The surface variable temperature is denoted by $T_w(x)$ while the surface variable concentration is $C_w(x)$. Uniform ambient temperature T_∞ and concentration C_∞ are experienced by the Maxwell fluid with $T_w > T_\infty$ and $C_w > C_\infty$ respectively. The particles concentration flux is assumed to be sufficiently small so that the thermophysical properties of relatively small number of particles will not affect the velocity and temperature distributions of the main stream. Constant particle diffusivity and sufficiently diluted particles concentration are assumed to prevent particles coagulation in the viscous flow region. Under these conventions with Boussineq's approximation, the boundary layer flow can be governed [11] as

$$\frac{\partial u}{\partial x} + \frac{\partial v}{\partial y} = 0, \tag{2.1}$$

$$u\frac{\partial u}{\partial x} + v\frac{\partial u}{\partial y} + \lambda_1 \left[u^2 \frac{\partial^2 u}{\partial x^2} + v^2 \frac{\partial^2 u}{\partial y^2} + 2uv \frac{\partial^2 u}{\partial x \partial y} \right]$$
$$= \nu \frac{\partial^2 u}{\partial y^2} - \frac{\nu}{K} u - \frac{\sigma B_0^2}{\rho} \left(u + \lambda_1 v \frac{\partial u}{\partial y} \right) + g[\beta_T(T - T_\infty) + \beta_C(C - C_\infty)], \tag{2.2}$$

$$u\frac{\partial T}{\partial x} + v\frac{\partial T}{\partial y} = \frac{\lambda_g}{\rho c_p}\frac{\partial^2 T}{\partial y^2} - \frac{1}{\rho c_p}\frac{\partial q_r}{\partial y} + \frac{Q_0}{\rho c_p}(T - T_\infty) + \frac{\mu}{\rho c_p}\left(\frac{\partial u}{\partial y}\right)^2 + \frac{\sigma B_0^2}{\rho c_p}u^2, \tag{2.3}$$

$$u\frac{\partial C}{\partial x} + v\frac{\partial C}{\partial y} = D\frac{\partial^2 C}{\partial y^2} - \frac{\partial(V_T C)}{\partial y}, \tag{2.4}$$

subject to the following boundary conditions

$$u = U_w(x) = ax, \quad v = 0, \quad T = T_w(x) = T_\infty + bx, \quad C = C_w(x) = C_\infty + cx, \text{ at } y = 0, \tag{2.5}$$

$$u \to 0, \quad \frac{\partial u}{\partial y} \to 0, \quad T \to T_\infty, \quad C \to C_\infty, \quad \text{as } y \to \infty, \tag{2.6}$$

with u and v are the x and y velocity components, λ_1 is the Maxwell relaxation time, μ is the dynamic viscosity, ν is the kinematic viscosity, ρ is the density of Maxwell fluid, K is the permeability of porous medium, σ is the electrical conductivity, g is the gravity acceleration, T is the fluid temperature, C is the concentration field, β_T is the temperature coefficient, β_C is the diluted volume coefficient, λ_g is the fluid thermal conductivity, c_p is the specific heat at constant pressure, Q_0 is the internal heat absorption, V_T is the thermophoretic velocity, D is the molecular diffusivity of species concentration, a is the rate of surface stretching while b and c are the coefficients for temperature and concentration gradients respectively.

Under Rosseland approximation, the thermal radiative transfer rate q_r [27] has the form

$$q_r = -\frac{4\sigma_1}{3k^*}\frac{\partial T^4}{\partial y}, \tag{2.7}$$

with σ_1 is Stefan-Boltzmann constant and k^* is a coefficient of mean absorption. From the second term in the RHS of the equation (2.3), the expression (2.7) will take positive value automatically. The differences in temperature throughout the flow are sufficiently small so it is permissible for T^4 to be expressed as a linear function of temperature [27],

$$T^4 \cong 4T_\infty{}^3 T - 3T_\infty{}^4. \tag{2.8}$$

Making use of equations (2.7)–(2.8), the equation (2.3) can then be utilized as

$$u\frac{\partial T}{\partial x} + v\frac{\partial T}{\partial y} = \frac{\lambda_g}{\rho c_p}\frac{\partial^2 T}{\partial y^2} + \frac{16\sigma_1 T_\infty{}^3}{3\rho c_p k^*}\frac{\partial^2 T}{\partial y^2} + \frac{Q_0}{\rho c_p}(T - T_\infty) + \frac{\mu}{\rho c_p}\left(\frac{\partial u}{\partial y}\right)^2 + \frac{\sigma B_0^2(x)}{\rho c_p}u^2. \tag{2.9}$$

Note that the second until the fifth terms in the RHS of (2.9) represent the expressions of thermal radiation, internal heat sink, viscous and magnetic heating respectively.

The thermophoresis effect is normally defined based on the mean velocity of a particle due to difference in temperature. Since the temperature gradient in the boundary layer is mainly reflected in the-y direction thus only the thermophoretic velocity in that direction should be focused on. Consequently, the thermophoretic velocity V_T which appears in (2.4) can be addressed as [27]:

$$V_T = -k\nu\frac{\nabla T}{T_{ref}} = -\frac{k\nu}{T_{ref}}\frac{\partial T}{\partial y}, \tag{2.10}$$

where T_{ref} is the control temperature whereas k is the coefficient for the thermophoretic velocity. The parameter of thermophoretic velocity, τ is now defined as follows [20]:

$$\tau = -\frac{k(T_w - T_\infty)}{T_{ref}}. \tag{2.11}$$

Typical values of $\tau = 0.01, 0.05, 0.1$ correspond to approximated values of $k(T_w - T_\infty) = 3K, 15K, 30K$ respectively for the control temperature $T_{ref} = 300K$. The negative sign in (2.11) refers to direction of particles velocity from a hot surface to a cooler surroundings. After similarity transformation is performed in the next section, the negative sign of the last term of the equation (2.16) will simultaneously impose the expression (2.11) to return only positive value.

2.2. Similarity equations

The governing equations (2.2)–(2.4) can be converted to a system of nonlinear ODES by adopting the non-dimensional variables as follow [11]:

$$\eta = \sqrt{\frac{a}{\nu}}y, \quad \psi = \sqrt{a\nu}xf(\eta), \quad \theta(\eta) = \frac{T - T_\infty}{T_w - T_\infty}, \quad \phi(\eta) = \frac{C - C_\infty}{C_w - C_\infty}, \tag{2.12}$$

where the stream function ψ fulfills (2.1) correctly when

$$u = \frac{\partial \psi}{\partial y} = axf'(\eta), \quad v = -\frac{\partial \psi}{\partial x} = -\sqrt{a\nu}f(\eta). \tag{2.13}$$

Using the equations (2.12) and (2.13), the transformed similarity equations and boundary conditions [11] are:

$$f''' + (1 + M^2\beta)ff'' - (f')^2 + 2\beta ff'f'' - \beta f^2 f''' - (\lambda + M^2)f' + \gamma[\theta + N\phi] = 0, \tag{2.14}$$

$$\left(1 + \frac{4}{3}R\right)\theta'' + \Pr(f\theta' - f'\theta) + \Pr\delta\theta + \Pr Ec(M^2f'^2 + f''^2) = 0, \tag{2.15}$$

$$\phi'' + Sc[f\phi' - f'\phi - \tau(\theta'\phi' + \theta''\phi)] = 0, \tag{2.16}$$

subject to

$$f(0) = 0, \quad f'(0) = 1, \quad \theta(0) = 1, \quad \phi(0) = 1, \quad \text{at } \eta = 0, \tag{2.17}$$
$$f' \to 0, \quad f'' \to 0, \quad \theta \to 0, \quad \phi \to 0, \quad \text{as } \eta \to \infty, \tag{2.18}$$

where $\beta = \lambda_1 a$ is the Maxwell relaxation time parameter also known as Deborah number, $M^2 = \sigma B_0^2/\rho a$ is the magnetic parameter, $\lambda = \nu/aK$ is the porosity parameter, $\gamma = Gr_x/Re_x^2$ is the local buoyancy parameter, $Gr_x = g\beta_T(T_w - T_\infty)x^3/\nu^2$ is the local Grashof number, $Re_x = U_w x/\nu$ is the local Reynolds number, $N = \beta_C(C_w - C_\infty)/\beta_T(T_w - T_\infty)$ is the ratio of volumetric expansion towards thermal expansion, $R = 4\sigma_1 T_\infty^3/k^*\lambda_g$ is the parameter for thermal radiation, $\Pr$ is the Prandtl number, $\delta = Q_0/\rho ac_p$ is the internal heat absorption parameter, $Ec = U_w^2/c_p(T_w - T_\infty)$ is the Eckert number and $Sc = \nu/D$ is the Schmidt number.

Hence, the local skin friction coefficient, local Nusselt number and local Sherwood number are defined as

$$Cf_x = \frac{2\tau_w}{\rho U_w^2}, \quad Nu_x = \frac{xq_w}{\lambda_g(T_w - T_\infty)}, \quad Sh_x = \frac{xj_w}{D(C_w - C_\infty)}, \tag{2.19}$$

in which the surface skin friction τ_w, the surface heat flux q_w and the surface mass flux j_w are given by

$$\tau_w = \mu\left(\frac{\partial u}{\partial y}\right)_{y=0}, \quad q_w = -\left(k + \frac{16\sigma_1 T_\infty^3}{3k^*}\frac{\partial T}{\partial y}\right)_{y=0}, \quad j_w = -D\left(\frac{\partial C}{\partial y}\right)_{y=0}. \tag{2.20}$$

Consequently the following non-dimensional variables can be obtained:

$$Cf_x Re_x^{\frac{1}{2}} = 2f''(0),$$

$$Nu_x Re_x^{-\frac{1}{2}}\left(\frac{3}{3 + 4R}\right) = -\theta'(0),$$

$$Sh_x Re_x^{-\frac{1}{2}} = -\phi'(0).$$

3. Numerical approach

The system of nonlinear higher order ordinary differential equations (2.14)–(2.16) subject to the conditions (2.17)–(2.18) is first solved using a shooting technique. Hence the following system is established after converting (2.14)–(2.16) into first order ordinary differential equations:

$$f' = p, \tag{3.1}$$

$$f'' = p' = q \tag{3.2}$$

$$f''' = p'' = q' = \frac{1}{(1 - \beta f^2)}[(f')^2 - (1 + M^2\beta)ff'' - 2\beta ff'f'' + (\lambda + M^2)f' - \gamma(\theta + N\phi)], \tag{3.3}$$

$$\theta' = r, \tag{3.4}$$

$$\theta'' = r' = \frac{3}{3 + 4R}[\Pr(f'\theta - f\theta') - \Pr\delta\theta - \Pr Ec(M^2 f'^2 + f''^2)], \tag{3.5}$$

$$\phi' = s, \tag{3.6}$$

$$\phi'' = s' = Sc[+f'\phi - f\phi' + \tau(\theta'\phi' + \theta''\phi)], \tag{3.7}$$

subject to the converted conditions of

$$f(0) = 0, \quad p(0) = 1, \quad \theta(0) = 1, \quad \phi(0) = 1, \text{ at } \eta = 0, \tag{3.8}$$

$$p \to 0, \quad q \to 0, \quad \theta \to 0, \quad \phi \to 0, \text{ as } \eta \to \infty. \tag{3.9}$$

For the purpose of solving (3.1)–(3.7) while satisfying the initial condition (3.8), the values of $q(0) = f''(0)$, $r(0) = \theta'(0)$ and $s(0) = \phi'(0)$ are required but not given initially. Therefore suitable guess values for $q(0)$, $r(0)$ and $s(0)$ are chosen so that further integration can be performed. Next, the calculated values for $p(\eta_{max}) = 0$, $q(\eta_{max}) = 0$, $\theta(\eta_{max}) = 0$ and $\phi(\eta_{max}) = 0$ at $\eta_{max} = 12$ (say) are compared with the boundary condition (3.9) while the estimated values of $q(0)$, $r(0)$ and $s(0)$ are adjusted to give better approximations for the solution. The classical Runge-Kutta method of fourth order with the step size $\Delta\eta = 0.01$ is employed and the previous process is repeated so that the asymptotically converged results can be achieved at 10^{-6} numeracy tolerance level.

4. Analytical solution

The expressions of velocity $f(\eta)$, temperature $\theta(\eta)$ and concentration $\phi(\eta)$ can be exemplified by the following base functions $\{\eta^l exp(-i\eta)|l, i \geq 0\}$ [16].

$$f(\eta) = a_{0,0} + \sum_{i=0}^{\infty}\sum_{l=0}^{\infty} a_{i,l}\eta^l e^{-i\eta}, \theta(\eta) = \sum_{i=0}^{\infty}\sum_{l=0}^{\infty} b_{i,l}\eta^l e^{-i\eta}, \phi(\eta) = \sum_{i=0}^{\infty}\sum_{l=0}^{\infty} c_{i,l}\eta^l e^{-i\eta}, \tag{4.1}$$

where $a_{i,l}, b_{i,l}$ and $c_{i,l}$ are the coefficients. The initial guesses f_0, θ_0 and ϕ_0 of $f(\eta), \theta(\eta)$ and $\phi(\eta)$ satisfying the solution rule [11] are

$$f_0(\eta) = 1 - e^{-\eta}, \quad \theta_0(\eta) = e^{-\eta}, \quad \phi_0(\eta) = e^{-\eta}. \tag{4.2}$$

The following auxiliary linear operators [11],

$$\mathcal{L}_f = \frac{\partial^3 f}{\partial\eta^3} - \frac{\partial f}{\partial\eta}, \quad \mathcal{L}_\theta = \frac{\partial^2\theta}{\partial\eta^2} - \theta, \quad \mathcal{L}_\phi = \frac{\partial^2\phi}{\partial\eta^2} - \phi \tag{4.3}$$

are chosen with the properties

$$\mathcal{L}_f[A_1 + A_2 e^{\eta} + A_3 e^{-\eta}] = 0, \quad \mathcal{L}_\theta[A_4 e^{\eta} + A_5 e^{-\eta}] = 0, \quad \mathcal{L}_\phi[A_6 e^{\eta} + A_7 e^{-\eta}] = 0, \tag{4.4}$$

where $A_j, (j = 1, .., 7)$ are the arbitrary constants.

If $\varsigma \in [0, 1]$ is the embedding parameter while $\hbar_f, \hbar_\theta$ and $\hbar_\phi$ are the nonzero auxiliary parameters such as $H_f(\eta), H_\theta(\eta)$ and $H_\phi(\eta)$ are the nonzero auxiliary functions respectively, then the zeroth order deformation equations [16] can be constructed as

$$(1 - \varsigma)\mathcal{L}_f[F(\eta; \varsigma) - f_0(\eta)] = \varsigma\hbar_f H_f(\eta)\mathcal{N}_f[F(\eta; \varsigma), \Theta(\eta; \varsigma), \Phi(\eta; \varsigma)], \tag{4.5}$$

$$(1 - \varsigma)\mathcal{L}_\theta[\Theta(\eta; \varsigma) - \theta_0(\eta)] = \varsigma\hbar_\theta H_\theta(\eta)\mathcal{N}_\theta[F(\eta; \varsigma), \Theta(\eta; \varsigma), \Phi(\eta; \varsigma)], \tag{4.6}$$

$$(1 - \varsigma)\mathcal{L}_\phi[\Phi(\eta; \varsigma) - \phi_0(\eta)] = \varsigma\hbar_\phi H_\phi(\eta)\mathcal{N}_\phi[F(\eta; \varsigma), \Theta(\eta; \varsigma), \Phi(\eta; \varsigma)], \tag{4.7}$$

subject to

$$F(0; \varsigma) = 0, \quad F'(0; \varsigma) = 1, \quad \Theta(0; \varsigma) = 1, \quad \Phi(0; \varsigma) = 1, F'(\infty; \varsigma) = 0, \quad \Theta(\infty; \varsigma) = 0, \quad \Phi(\infty; \varsigma) = 0. \tag{4.8}$$

The nonlinear operators $\mathcal{N}_f, \mathcal{N}_\theta$ and $\mathcal{N}_\phi$ are

$$\begin{aligned}\mathcal{N}_f[F(\eta; \varsigma), \Theta(\eta; \varsigma), \Phi(\eta; \varsigma)] =& F'''(\eta; \varsigma) + (1 + M^2\beta)F(\eta; \varsigma)F''(\eta; \varsigma) - [F'(\eta; \varsigma)]^2 \\ &- (\lambda + M^2)F'(\eta; \varsigma) + 2\beta F(\eta; \varsigma)F'(\eta; \varsigma)F''(\eta; \varsigma) \\ &- \beta[F(\eta; \varsigma)]^2 F'''(\eta; \varsigma) + \gamma[\Theta(\eta; \varsigma) + N\Phi(\eta; \varsigma)],\end{aligned} \tag{4.9}$$

$$\begin{aligned}\mathcal{N}_\theta[F(\eta; \varsigma), \Theta(\eta; \varsigma), \Phi(\eta; \varsigma)] =& \left(1 + \frac{4}{3}R\right)\Theta''(\eta; \varsigma) + \Pr \delta\Theta(\eta; \varsigma) \\ &+ \Pr[F(\eta; \varsigma)\Theta'(\eta; \varsigma) - F'(\eta; \varsigma)\Theta(\eta; \varsigma)] \\ &+ Ec[[F''(\eta; \varsigma)]^2 + M^2[F'(\eta; \varsigma)]^2]],\end{aligned} \tag{4.10}$$

$$\begin{aligned}\mathcal{N}_\phi[F(\eta; \varsigma), \Theta(\eta; \varsigma), \Phi(\eta; \varsigma)] =& \Phi''(\eta; \varsigma) + Sc[F(\eta; \varsigma)\Phi'(\eta; \varsigma) - F'(\eta; \varsigma)\Phi(\eta; \varsigma)] \\ &- Sc\tau[\Theta'(\eta; \varsigma)\Phi'(\eta; \varsigma) + \Theta''(\eta; \varsigma)\Phi(\eta; \varsigma)].\end{aligned} \tag{4.11}$$

When $\varsigma = 0$ and $\varsigma = 1$, we have

$$F(\eta; 0) = f_0(\eta), \quad F(\eta; 1) = f(\eta), \tag{4.12}$$

$$\Theta(\eta; 0) = \theta_0(\eta), \quad \Theta(\eta; 1) = \theta(\eta), \tag{4.13}$$

$$\Phi(\eta; 0) = \phi_0(\eta), \quad \Phi(\eta; 1) = \phi(\eta). \tag{4.14}$$

$F(\eta; \varsigma), \Theta(\eta; \varsigma)$ and $\Phi(\eta; \varsigma)$ can be expanded in terms of Taylor series of ς [16],

$$F(\eta; \varsigma) = f_0(\eta) + \sum_{l=1}^{+\infty} f_l(\eta)\varsigma^l, \tag{4.15}$$

$$\Theta(\eta; \varsigma) = \theta_0(\eta) + \sum_{l=1}^{+\infty} \theta_l(\eta)\varsigma^l, \tag{4.16}$$

$$\Phi(\eta; \varsigma) = \phi_0(\eta) + \sum_{l=1}^{+\infty} \phi_l(\eta)\varsigma^l, \tag{4.17}$$

before the $[n, n]$ Padé-approximants can be generated where

$$f_l(\eta) = \frac{1}{l!}\left[\frac{\partial^l F(\eta; \varsigma)}{\partial \varsigma^l}\right]_{\varsigma=0}, \tag{4.18}$$

$$\theta_l(\eta) = \frac{1}{l!}\left[\frac{\partial^l \Theta(\eta; \varsigma)}{\partial \varsigma^l}\right]_{\varsigma=0}, \tag{4.19}$$

$$\phi_l(\eta) = \frac{1}{l!}\left[\frac{\partial^l \Phi(\eta; \varsigma)}{\partial \varsigma^l}\right]_{\varsigma=0}. \tag{4.20}$$

In order for the deformation equations (4.5)–(4.7) to converge at $\varsigma = 1$, the auxiliary parameters and functions must be properly chosen [16]:

$$f(\eta) = f_0(\eta) + \sum_{l=1}^{+\infty} f_l(\eta), \tag{4.21}$$

$$\theta(\eta) = \theta_0(\eta) + \sum_{l=1}^{+\infty} \theta_l(\eta), \tag{4.22}$$

$$\phi(\eta) = \phi_0(\eta) + \sum_{l=1}^{+\infty} \phi_l(\eta). \tag{4.23}$$

The mth-order deformation equations can now be obtained as follows [16]:

$$\mathcal{L}_f[f_m(\eta) - \chi_m f_{m-1}(\eta)] = \hbar_f H_f(\eta) \mathcal{R}_m^f(\eta), \tag{4.24}$$

$$\mathcal{L}_\theta[\theta_m(\eta) - \chi_m \theta_{m-1}(\eta)] = \hbar_\theta H_\theta(\eta) \mathcal{R}_m^\theta(\eta), \tag{4.25}$$

$$\mathcal{L}_\phi[\phi_m(\eta) - \chi_m \phi_{m-1}(\eta)] = \hbar_\phi H_\phi(\eta) \mathcal{R}_m^\phi(\eta), \tag{4.26}$$

subject to

$$f_m(0) = 0, \quad f'_m(0) = 0, \quad \theta_m(0) = 0, \quad \phi_m(0) = 0, \quad f'_m(\infty) = 0, \quad \theta_m(\infty) = 0, \quad \phi_m(\infty) = 0 \tag{4.27}$$

for $m \geq 1$, where

$$\mathcal{R}_m^f(\eta) = f'''_{l-1} - (\lambda + M^2)f'_{l-1} + \sum_{i=0}^{l-1}[(1 + M^2\beta)f_i f''_{l-1-i} - f'_i f'_{l-1-i}]$$
$$+ 2\beta \sum_{i=0}^{l-1} \sum_{k=0}^{i} f_k f'_{i-k} f''_{l-1-i} - \beta \sum_{i=0}^{l-1} \sum_{k=0}^{i} f_k f_{i-k} f'''_{l-1-i} + \gamma(\theta_{l-1} + N\phi_{l-1}), \tag{4.28}$$

$$\mathcal{R}_m^\theta(\eta) = \left(1 + \frac{4}{3}R\right)\theta''_{l-1} + \Pr \sum_{i=0}^{l-1}[f_i \theta'_{l-1-i} - f'_{l-1-i}\theta_i] + \Pr \delta\theta_{l-1}$$
$$+ \Pr Ec \sum_{i=0}^{l-1}[M^2 f'_i f'_{l-1-i} + f''_i f''_{l-1-i}], \tag{4.29}$$

$$\mathcal{R}_m^\phi(\eta) = Sc \sum_{i=0}^{l-1}[f_i \phi'_{l-1-i} - f'_{l-1-i}\phi_i] - Sc\tau \sum_{i=0}^{l-1}[\theta'_i \phi'_{l-1-i} + \theta''_{l-1-i}\phi_i] + \phi''_{l-1} \tag{4.30}$$

and

$$\chi_m = \begin{cases} 0, & m \leq 1 \\ 1, & m > 1. \end{cases}$$

The solutions for the mth-order deformation equations can now be expressed as

$$f_m(\eta) = f_m^*(\eta) + A_1 + A_2 e^\eta + A_3 e^{-\eta}, \tag{4.31}$$

$$\theta_m(\eta) = \theta_m^*(\eta) + A_4 e^\eta + A_5 e^{-\eta}, \tag{4.32}$$

$$\phi_m(\eta) = \phi_m^*(\eta) + A_6 e^\eta + A_7 e^{-\eta}, \tag{4.33}$$

where

$$A_2 = A_4 = A_6 = 0, A_1 = -A_3 - f_m^*(0), \quad A_3 = \left[\frac{\partial f_m^*(\eta)}{\partial \eta}\right]_{\eta=0}, A_5 = -\theta_m^*(0), \quad A_7 = -\phi_l^*(0),$$

and $f_m^*(\eta)$, $\theta_m^*(\eta)$, $\phi_m^*(\eta)$ are the resulting equations from the multiple integration process.

5. Results and discussion

The reliability of homotopy analysis method is mainly dependent on convergence control parameter $\hbar$. In HAM, proper value of this parameter is defined when the $\hbar$ curve is horizontally straight such that values of the reduced skin friction coefficient, Nusselt number and Sherwood number become almost stagnant in the y-direction of the graph. Since this method consumes time, we employ the homotopy-Padé technique to speed up the convergence of the HAM solutions (4.31)–(4.33). The results are generated in the form of a fraction with one polynomial of order η^n in the numerator and another polynomial of order η^n in the denominator. The algorithm for solving the equations (4.24)–(4.27) is coded in Mathematica software. In all computations done, the auxiliary functions $H_f(\eta) = 1$, $H_\theta(\eta) = 1$ and $H_\phi(\eta) = 1$ are considered. The single auxiliary parameter $\hbar$ is introduced to represent the values of $\hbar_f, \hbar_\theta$ and $\hbar_\phi$, i.e. $\hbar = \hbar_f = \hbar_\theta = \hbar_\phi$. Based on Fig. 2 when $\beta = \tau = 0.2$, $M = \gamma = N = \lambda = 1$, Pr $= 3$, $Sc = Ec = 0.5$, $R = 0.3$ and $\delta = -1$ respectively, better convergent values can be taken within the close range of $-0.3 \leq \hbar \leq -0.2$ in conventional HAM. On top of that, if the optimal value of $\hbar$ is to be selected using the optimal homotopy analysis method, it can be done by minimizing the summation of the discrete squared residual of the governing equations (2.14)–(2.16), [19].
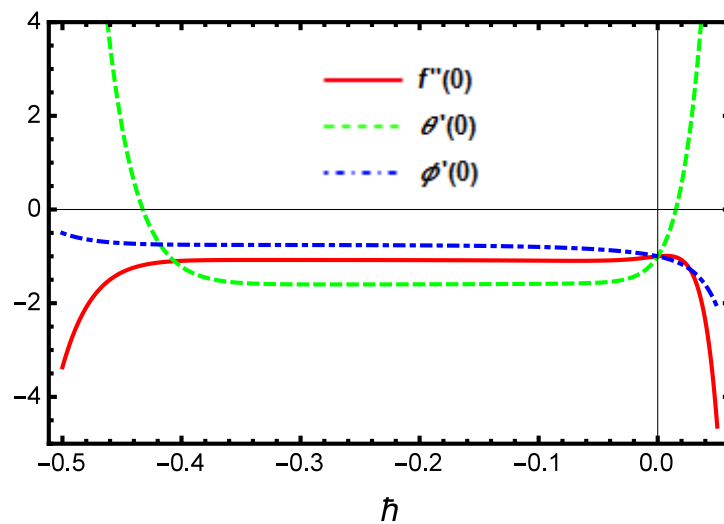

Figure 2: The $\hbar$ curves for $f''(0)$, $\theta'(0)$ and $\phi'(0)$ using the 20th-order HAM for the case $\beta = \tau = 0.2$, $M = \lambda = \gamma = N = 1$, Pr $= 3$, $Sc = Ec = 0.5$, $R = 0.3$ and $\delta = -1$ respectively.

The present numerical result and the accelerated convergence of the homotopy solutions via Padé approximation are presented in Table 1. Since we have calculated the HAM solutions with 74 terms, it is possible to obtain up to [37, 37] homotopy-Padé scheme. Note that at the [30, 30] order when Pr $= 10$, all solutions converge to the [37, 37] order of homotopy-Padé within six significant figures. On the other hand, the present values of $-f''(0)$ obtained using shooting-RK4 method and [20, 20] homotopy-Padé scheme are compared with numerical results produced by [1] and [22] in Table 2 when Hartmann number, porosity and buoyancy parameters are equal to zero while Maxwell parameter is varied. These values agree with each other up to five significant figures possibly due to discrepancy between numerical and analytical methods employed. More results of wall skin friction, wall heat flux and wall mass flux are tabulated in Table 3 and Table 4 for variations in Hartmann number, ratio of volumetric towards thermal expansions, porosity, thermophoresis, radiation and heat absorption respectively. As M or λ increases, the values of $-f''(0)$ increase while $-\theta'(0)$ and $-\phi'(0)$ decrease. Opposite effects are accomplished by the ratio of volumetric-thermal expansions N while thermophoresis replicates the qualitative influences of M and λ with exception on the wall mass transfer $-\phi'(0)$. Eventually, thermal radiation R and heat sink δ cause all values of $-f''(0)$, $-\theta'(0)$ and $-\phi'(0)$ to decline as showed in Table 4.

Table 1: The $[n, n]$ homotopy-Padé approximations when $\tau = \beta = 0.2$, $M = \lambda = N = \gamma = 1$, Pr $= 10$, $Ec = Sc = 0.5$, $R = 0.3$ and $\delta = -1$.

$[n, n]$	$-f''(0)$	$-\theta'(0)$	$-\phi'(0)$
$[5, 5]$	1.1559440	2.5949672	0.76014478
$[10, 10]$	1.1435399	2.6296448	0.84408154
$[15, 15]$	1.1420161	2.6341925	0.84158538
$[20, 20]$	1.1419568	2.6344352	0.8409284
$[25, 25]$	1.1419520	2.6344877	0.8409083
$[30, 30]$	1.1419488	2.6344904	0.8409055
$[35, 35]$	1.1419483	2.6344911	0.8409050
$[36, 36]$	1.1419483	2.6344911	0.8409049
$[37, 37]$	1.1419483	2.6344911	0.8409049
Numerical	1.1419812	2.6344318	0.8409742

Table 2: The values of $-f''(0)$ when $M = \lambda = \gamma = 0$ and β is varied.

β	Ref.[1]	Ref.[22]	Present Results	
			Numerical	[20,20] HAM-Padé
0.0	0.999962	0.999963	1.000000	1.000000
0.2	1.051948	1.051949	1.051890	1.051890
0.4	1.101850	1.101851	1.101904	1.101903
0.6	1.150163	1.150162	1.150143	1.150137
0.8	1.196692	1.196693	1.196722	1.196711

Table 3: The values of $f''(0)$, $\theta'(0)$ and $\phi'(0)$ when $\tau = 0.2$, $\gamma = 1$, Pr $= 3$, $Sc = Ec = 0.5$, $\beta = R = 0.3$ and $\delta = -1$ using numerical method and $[20, 20]$ homotopy-Padé scheme.

M	N	λ	Numerical			[20,20] HAM-Padé		
			$-f''(0)$	$-\theta'(0)$	$-\phi'(0)$	$-f''(0)$	$-\theta'(0)$	$-\phi'(0)$
0	1	1	0.730603	2.013695	0.841720	0.730511	2.013780	0.841607
0.5	1	1	0.829239	1.899656	0.816404	0.829132	1.899750	0.816236
1	0	1	1.511944	1.380897	0.619069	1.511944	1.380897	0.614536
1	0.5	1	1.299346	1.500350	0.698009	1.299270	1.500410	0.697227
1	1	0	0.738269	1.703249	0.808438	0.738146	1.703310	0.808331
1	1	0.5	0.927704	1.647621	0.777160	0.927559	1.647720	0.776932
1	1	1	1.099996	1.589807	0.748344	1.099660	1.589860	0.747996

Table 4: The values of $f''(0)$, $\theta'(0)$ and $\phi'(0)$ when $\beta = 0.3$, $M = N = \lambda = \gamma = 1$, Pr $= 3$ and $Sc = Ec = 0.5$ using numerical method and $[20, 20]$ homotopy-Padé scheme.

τ	R	δ	Numerical			[20,20] HAM-Padé		
			$-f''(0)$	$-\theta'(0)$	$-\phi'(0)$	$-f''(0)$	$-\theta'(0)$	$-\phi'(0)$
0.2	0.3	-1	1.099996	1.589807	0.748344	1.099660	1.589860	0.747996
0.5	0.3	-1	1.120546	1.577188	0.938601	1.120373	1.577337	0.938226
1	0.3	-1	1.152192	1.557277	1.257871	1.152013	1.557439	1.257486
1	0.5	-1	1.138839	1.448185	1.209956	1.138663	1.448309	1.209572
1	1	-3	1.183650	1.973015	1.451393	1.183460	1.973090	1.450862
1	1	-2	1.154788	1.648550	1.302678	1.154604	1.648647	1.302269
1	1	-1	1.112279	1.254950	1.127236	1.112115	1.255062	1.126862

The effects of Maxwell relaxation time parameter β, Hartmann number M, porosity λ, buoyancy γ, ratio of volumetric-thermal expansions N, thermal radiation R, Prandtl number Pr, internal heat sink δ, Eckert number Ec, Schmidt number Sc and thermophoresis τ towards the velocity, temperature and concentration profiles are revealed in Fig. 3 and Fig. 4 respectively. The physical behaviors demonstrated in these figures are conforming the values of wall skin friction, wall heat flux and wall mass flux as enlisted in Table 3 and Table 4. Based on Fig. 3(a), no significant effect of β is detected on the temperature profile. The flow velocity declines with an increment in M as the applied transverse magnetic field produces a Lorentz drag force in the opposite direction of the flow. Consequently, this phenomenon induces a slight hike in the temperature profile due to Lorentz force addendum on the existing skin friction implies more heat to be transferred from the wall thus heating the flow. These low velocity, high friction and low temperature on the wall also contribute to increasing mass deposition on the surface. The same consequences of M are postulated by λ in Fig. 3(b) but due to porosity interference in the flow direction. Adversely greater buoyancy γ assists the flow dynamics and cooling while avoiding concentration build-up near the surface area. As thermal radiation R proliferates in Fig. 3(c), the flow is streaming and cooling down at a slower rate leading to faster concentration reduction from the wall. Similar behaviors are observed for expansion ratio N except for the flow temperature where the effect is slightly reversed.
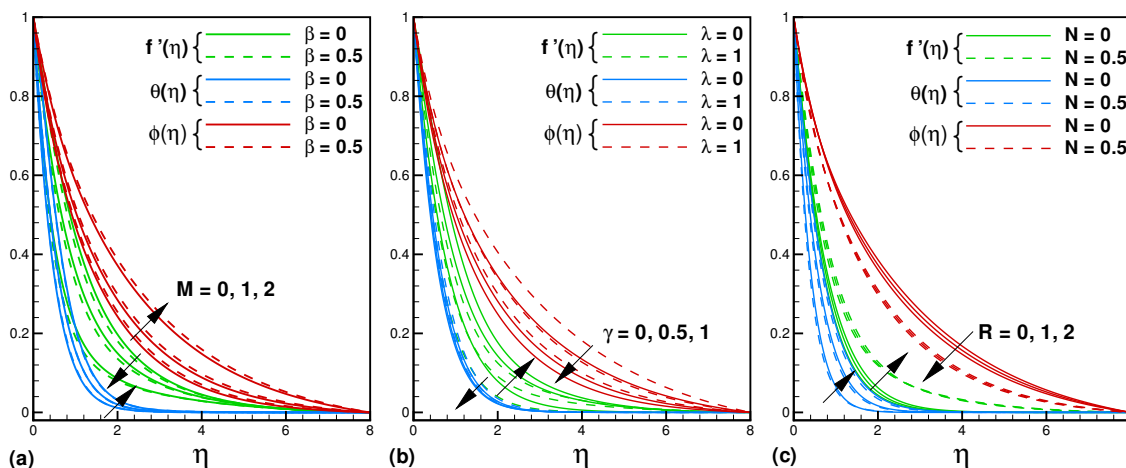

Figure 3: The flow profiles under influences of (a) Hartmann number, (b) buoyancy and (c) thermal radiation when $\tau = 0.2$, $\beta = R = 0.3$, $\lambda = \gamma = 1$, Pr $= 3$, $M = N = Sc = Ec = 0.5$ and $\delta = -1$ respectively.
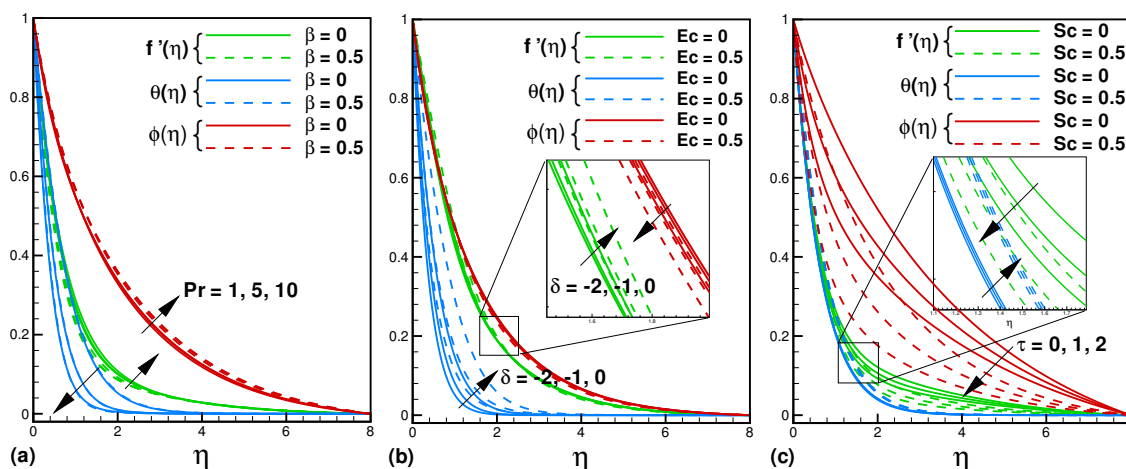

Figure 4: The flow profiles under influences of (a) Prandtl number, (b) heat sink and (c) thermophoresis when $\tau = 0.2$, $\lambda = M = N = 1$, Pr $= 3$, $\beta = \gamma = R = Sc = Ec = 0.5$ and $\delta = -1$ respectively.

Prandtl number represents diffusivity ratio of momentum towards energy while a heat sink is a mechanism that cools a medium by dissipating heat to surroundings. The differences between a heat source and a heat sink lie in the opposite sign of the values and in the opposite directions of the progress impact. As the value of δ moves closer towards negative axial plane, the effect of heat absorption will come into practice. On the other hand, thermophoresis tends to drive away mass deposition from the wall surface of temperature T_w which is hotter than the surroundings. Based on Fig. 4, all velocity profiles increase with Prandtl number Pr, Eckert number Ec and heat sink δ. Since these parameters (excluding β) affect directly the heat equation (2.15), primary discussions can be focalized on temperature and concentration profiles. With higher value of Pr, momentum diffusivity becomes greater than thermal diffusivity. Therefore the flow temperature slightly declines while the concentration is improved. When the value of δ approaching zero or a positive number, the role of internal heat sink transforms into a heat source factor causing the flow temperature to hike and lowering the concentration level. On the other hand, warmer temperature in the flow promotes higher migration of diluted particles to cooler surroundings thus lessening the fluid concentration near the plate with an increment in thermophoresis. Apparently Eckert and Schmidt numbers have similar effects towards fluid flow extra heating and lower concentration.

The profiles of reduced skin friction coefficient $Cf_x Re_x^{\frac{1}{2}}$, reduced Nusselt number $Nu_x Re_x^{-\frac{1}{2}}$ and reduced Sherwood number $Sh_x Re_x^{-\frac{1}{2}}$ under influence of internal heat absorption parameter δ, thermal radiation parameter R, Eckert number Ec, Maxwell relaxation time parameter β, buoyancy parameter γ, expansion ratio N, thermophoresis parameter τ and Schmidt number Sc are illustrated in Figs. 5–9 respectively. Thermal radiation is a type of non-ionizing radiation that radiates through space where the thermal energy is conserved in a vacuum. Conventionally, it is considered as harmless as long as extreme temperature rise is not produced. From Fig. 5, it is evidenced that as thermal radiation increases, the reduced Nusselt number is multiplied while the reduced skin friction coefficient and the reduced Sherwood number decline. Obviously, both internal heat source (by taking positive values of heat absorption parameter) and Eckert number contribute to significant reduction of the three physical quantities $Cf_x Re_x^{\frac{1}{2}}$, $Nu_x Re_x^{-\frac{1}{2}}$ and $Sh_x Re_x^{-\frac{1}{2}}$ as depicted in Fig. 6. Based on Fig. 5(b) and Fig. 6(b), it is found that the heat transfer performance is progressively advanced as the negative sign of the internal heat absorption value is intensified.
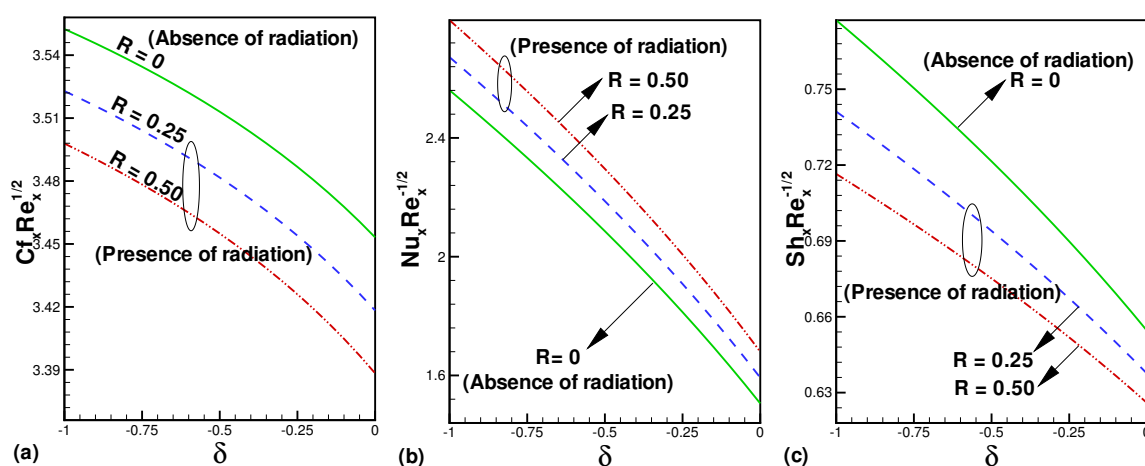

Figure 5: The effects of thermal radiation R and internal heat sink δ on (a) reduced skin friction coefficient, (b) reduced Nusselt number and (c) reduced Sherwood number when $\beta = \lambda = \tau = M = \gamma = N = Ec = 0.5$, Pr $= 5$, $Sc = 0.25$ respectively.
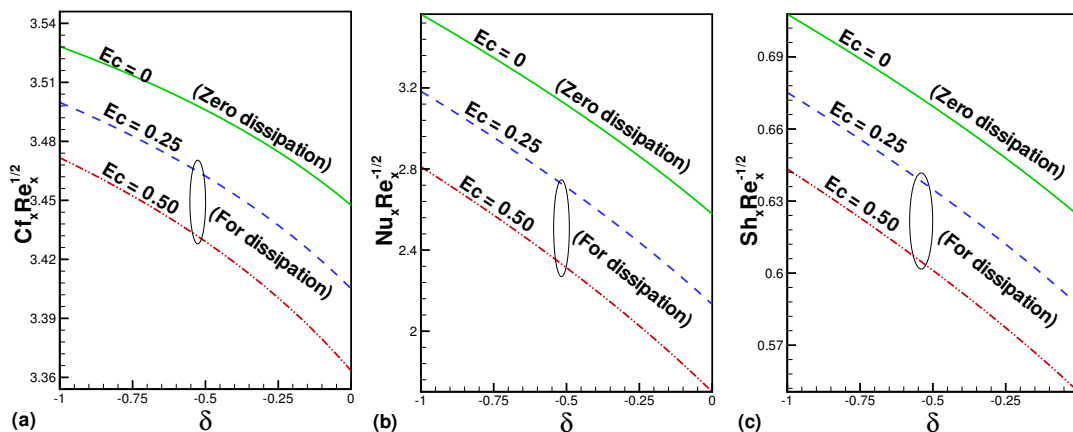
Figure 6: The effects of Eckert number Ec and internal heat sink δ on (a) reduced skin friction coefficient, (b) reduced Nusselt number and (c) reduced Sherwood number when $\beta = \lambda = \tau = M = \gamma = N = R = Sc = 0.5$, $\Pr = 5$, $Sc = 0.25$ respectively.
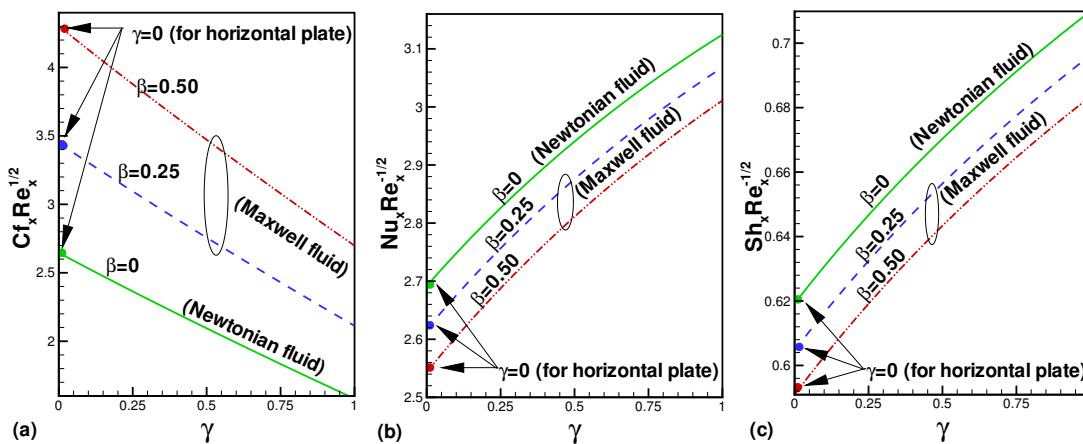

Figure 7: The effects of Maxwell parameter β and buoyancy parameter γ on (a) reduced skin friction coefficient, (b) reduced Nusselt number and (c) reduced Sherwood number when $\beta = \lambda = \tau = M = N = R = Ec = 0.5$, $\Pr = 5$, $Sc = 0.25$, $\delta = -1$ respectively.
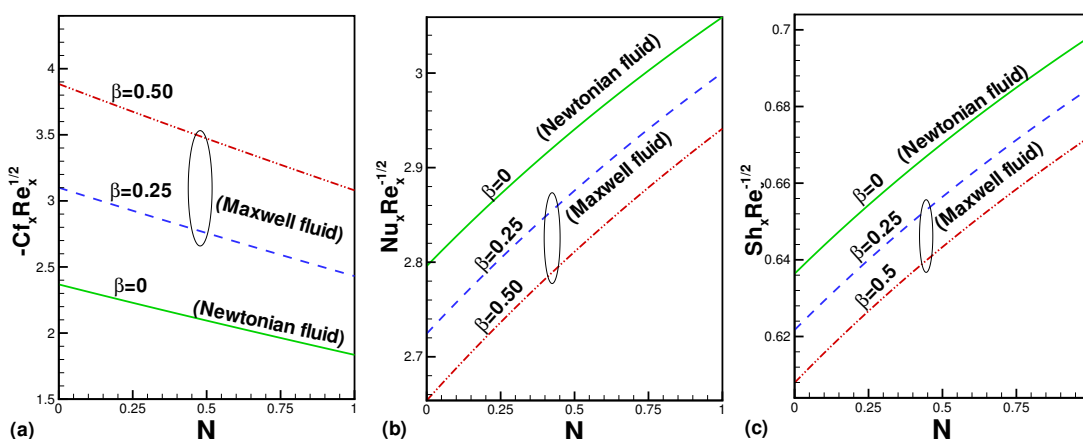

Figure 8: The effects of Maxwell parameter β and ratio of volumetric-thermal expansion N on (a) reduced skin friction coefficient, (b) reduced Nusselt number and (c) reduced Sherwood number when $\beta = \lambda = \tau = M = \gamma = R = Ec = 0.5$, $\Pr = 5$, $Sc = 0.25$, $\delta = -1$ respectively.
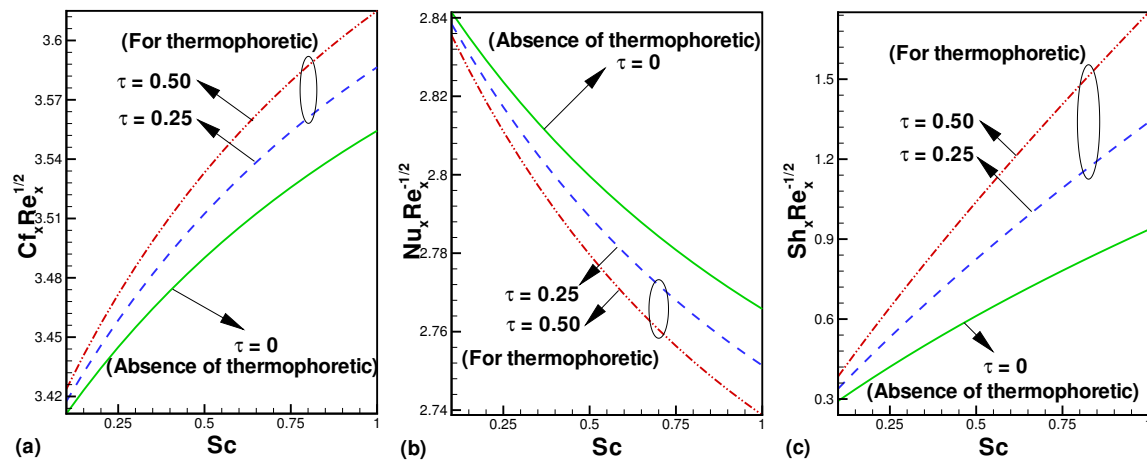
Figure 9: Influence of thermophoresis and Schmidt number Sc on reduced (a) skin friction, (b) Nusselt number and (c) Sherwood number when $\beta = M = N = \lambda = \gamma = R = Sc = Ec = 0.5$, $\Pr = 5$, $\delta = -1$ respectively.

Maxwell relaxation time parameter, β is an important factor that sets apart the characteristics between a general Newtonian fluid as compared to the Maxwell fluid which represents a rate-type of non-Newtonian fluid. Due to an increase in shear stress property of non-Newtonian fluid towards it's motion, the layer of the fluid molecules becomes slightly sticky and the fluid dynamics is slower due to relaxation period is increased and the flow can now hold sufficiently minimum extra pressure for a bit longer time. The impacts of β in stimulating higher reduced skin friction coefficient as opposed to the flow direction while deflating the heat and mass fluxes are in contrast consequence with buoyancy γ and volumetric-thermal expansion ratio N as demonstrated in Fig. 7 and Fig. 8 respectively. With greater friction and lower rate of transfer of heat and mass amounts from the plate, the cooler plate becomes a proper bedding for attracting higher deposition of diluted micro and nano scaled particles due to accumulating thermophoresis and Schmidt number as revealed in Fig. 9. Finally the streamlines in Fig. 10 provide a snapshot of the flow field characteristics in comparison between a general Newtonian fluid ($\beta = 0$) and the Maxwell non-Newtonian fluid ($\beta \neq 0$) as the relaxation time parameter is varied.
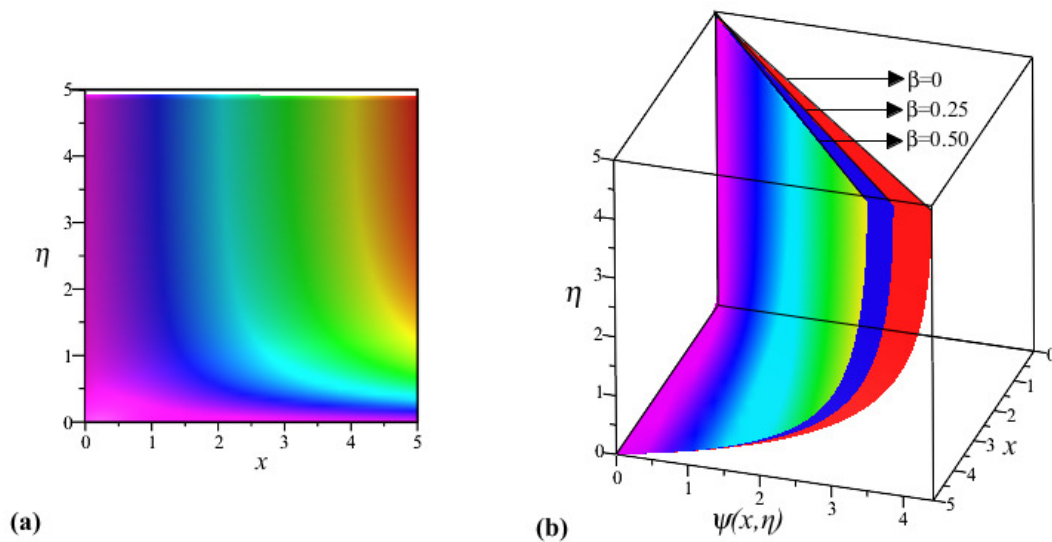

Figure 10: The flow streamlines in (a) two dimensions and (b) three dimensions when Maxwell parameter is varied.

6. Concluding remarks

In this study, the influence of internal heat sink as heat dissipating mechanism in the Maxwell fluid flow past a vertical sheet has been considered. The set of governing equations has been transformed to ordinary differential equations by means of similarity variables before they are solved using the shooting-RK4 method validated with homotopy-Padé series acceleration. The present numerical and analytical solutions agree to each other up to three significant figures at minimum. The profiles of velocity, temperature and concentration distributions for selected variation of the flow parameters are also presented along with graphical results of reduced skin friction coefficient, reduced Nusselt number and reduced Sherwood number. The following points are concluded:

- The buoyancy parameter γ assists the flow dynamics and cooling while avoiding concentration build-up near the surface area.

- As thermal radiation R proliferates, the flow is streaming and cooling down at a slower rate leading to faster concentration reduction from the wall.

- As thermal radiation increases, the reduced Nusselt number is multiplied while the reduced skin friction coefficient and the reduced Sherwood number decline.

- All velocity profiles increase with Prandtl number Pr, Eckert number Ec and heat sink δ.

- With higher value of Pr, the flow temperature slightly declines while the concentration is improved.

- When the value of δ approaching zero or positive number, the role of internal heat sink transforms into a heat source factor causing the flow temperature to hike and lowering the concentration level.

- It is found that the heat transfer performance is progressively advanced as the internal heat absorption δ holds greater value in the negative axial direction.

- Warmer temperature in the flow promotes higher migration of diluted particles to cooler surroundings thus lessening the fluid concentration near the plate with an increment in thermophoresis.

- Eckert and Schmidt numbers contribute similar effects towards fluid flow extra heating and lower concentration.

- Both internal heat source and Eckert number contribute to significant reduction of the skin friction coefficient, reduced Nusselt number and reduced Sherwood number.

- The impacts of Maxwell relaxation time parameter β in stimulating higher reduced skin friction coefficient in the flow direction while deflating the heat and mass fluxes are in contrast consequence with buoyancy γ and volumetric-thermal expansion ratio N.

- With greater friction and lower rates of heat and mass transfers, the cooler plate is attracting higher deposition of diluted micro and nano scaled particles due to accumulating thermophoresis and Schmidt number.

Acknowledgements

References

[1] M. S. Abel, J. V. Tawade, M. M. Nandeppanavar, *MHD flow and heat transfer for the upper-convected Maxwell fluid over a stretching sheet*, Meccanica, **47** (2012), 385–393. 1, 5, 2

[2] A. Einstein, *Does the inertia of a body depend upon its energy-content?*, Annalen der Physik, **18** (1905), 639–641. 1

[3] C. Fetecau, M. Athar, C. Fetecau, *Unsteady flow of a generalized Maxwell fluid with fractional derivative due to a constantly accelerating plate*, Comput. Math. Appl., **57** (2009), 596–603. 1

[4] C. Fetecau, C. Fetecau, *The Rayleigh-Stokes-problem for a fluid of Maxwellian type*, Int. J. Non-Linear Mech., **38** (2003), 603–607. 1

[5] C. Fetecau, C. Fetecau, *A new exact solution for the flow of a Maxwell fluid past an infinite plate*, Int. J. Non-Linear Mech., **38** (2003), 423–427. 1

[6] S. L. Goren, *Thermophoresis of aerosol particles in laminar boundary layer on a flat plate*, J. Colloid Interface Sci., **61** (1977), 77–85. 1

[7] F. Guerrero, F. J. Santonja, R. J. Villanueva, *Solving a model for the evolution of smoking habit in Spain with homotopy analysis method*, Nonlinear Anal. Real World Appl., **14** (2013), 549–558. 1

[8] H. N. Hassan, M. A. El-Tawil, *A new technique of using homotopy analysis method for second order nonlinear differential equations*, Appl. Math. Comput., **219** (2012), 708–728. 1

[9] T. Hayat, Z. Abbas, N. Ali, *MHD flow and mass transfer of a upper-convected Maxwell fluid past a porous shrinking sheet with chemical reaction species*, Phys. Lett. A, **372** (2008), 4698–4704. 1

[10] T. Hayat, M. Awais, M. Qasim, A. A. Hendi, *Effects of mass transfer on the stagnation point flow of an upper-convected Maxwell (UCM) fluid*, Int. J. Heat Mass Transf., **54** (2011), 3777–3782. 1

[11] T. Hayat, M. Qasim, *Influence of thermal radiation and Joule heating on MHD flow of a Maxwell fluid in the presence of thermophoresis*, Int. J. Heat Mass Transf., **53** (2010), 4780–4788. 1, 2.1, 2.2, 2.2, 4, 4

[12] T. Hayat, M. Sajid, *Homotopy analysis of MHD boundary layer flow of an upper-convected Maxwell fluid*, Int. J. Eng. Sci., **45** (2007), 393–401. 1

[13] T. Hayat, R. Sajjad, Z. Abbas, M. Sajid, A. A. Hendi, *Radiation effects on MHD flow of Maxwell fluid in a channel with porous medium*, Int. J. Heat Mass Transf., **54** (2011), 854–862. 1

[14] R. Kandasamy, I. Muhaimin, H. Bin Saim, *Lie group analysis for the effect of temperature-dependent fluid viscosity with thermophoresis and chemical reaction on MHD free convective heat and mass transfer over a porous stretching surface in the presence of heat source/sink*, Commun. Nonlinear Sci. Numer. Simul., **15** (2010), 2109–2123. 1

[15] M. H. Kargarnovin, S. A. Faghidian, Y. Farjami, G. H. Farrahi, *Application of homotopy-Pad technique in limit analysis of circular plates under arbitrary rotational symmetric loading using von-Mises yield criterion*, Commun. Nonlinear Sci. Numer. Simul., **15** (2010), 1080–1091. 1

[16] S. J. Liao, *Beyond Perturbation: Introduction to the Homotopy Analysis Method*, Chapman and Hall, Boca Raton, (2004). 1, 4, 4, 4, 4, 4

[17] S. J. Liao, *A new branch of solutions of boundary-layer flows over an impermeable stretched plate*, Int. J. Heat Mass Transf., **48** (2005), 2529–2539. 1

[18] S. J. Liao, *An optimal homotopy-analysis approach for strongly nonlinear differential equations*, Commun. Nonlinear Sci. Numer. Simul., **15** (2010), 2003–2016. 1

[19] S. J. Liao, *Homotopy analysis method in nonlinear differential equations*, Higher Education Press and Springer, Beijing and Heidelberg, (2012). 1, 5

[20] A. F. Mills, X. Hang, F. Ayazi, *The effect of wall suction and thermophoresis on aerosol-particle deposition from a laminar boundary layer on a flat plate*, Int. J. Heat Mass Transf., **27** (1984), 1110–1113. 2.1

[21] S. S. Motsa, P. Sibanda, S. Shateyi, *A new spectral-homotopy analysis method for solving a nonlinear second order BVP*, Commun. Nonlinear Sci. Numer. Simul., **15** (2010), 2293–2302. 1

[22] S. Mukhopadhyay, *Heat transfer analysis of the unsteady flow of a Maxwell fluid over a stretching surface in the presence of a heat source/sink*, Chinese Phys. Lett., **29** (2012), 12 pages. 1, 5, 2

[23] N. F. M. Noor, O. Abdulaziz, I. Hashim, *MHD fow and heat transfer in a thin liquid film on an unsteady stretching sheet by the homotopy analysis method*, Int. J. Numer. Methods Fluids, **63** (2010), 357–373. 1

[24] N. F. M. Noor, S. Abbasbandy, I. Hashim, *Heat and mass transfer of thermophoretic MHD flow over an inclined radiate isothermal permeable surface in the presence of heat source/sink*, Int. J. Heat Mass Transf., **55** (2012), 2122–2128. 1

[25] K. Sadeghy, A. H. Najafi, M. Saffaripour, *Sakiadis flow of an upper-convected Maxwell fluid*, Int. J. Non-Linear Mech., **40** (2005), 1220–1228. 1

[26] M. Shaban, S. Kazem, J. A. Rad, *A modification of the homotopy analysis method based on Chebyshev operational matrices*, Math. Comput. Modelling, **57** (2013), 1227–1239. 1

[27] L. Talbot, R. K. Cheng, A. W. Schefer, D. R. Wills, *Thermophoresis of particles in a heated boundary layer*, J. Fluid Mech., **101** (1980), 737–758. 2.1, 2.1, 2.1

[28] Y. Wang, T. Hayat, *Fluctuating flow of a Maxwell fluid past a porous plate with variable suction*, Nonlinear Anal. Real World Appl., **9** (2008), 1269–1282. 1

[29] H. Xu, S. J. Liao, *A series solution of the unsteady Von Karman swirling viscous flows*, Acta Appl. Math., **94** (2006), 215–231. 1